J. Fluid Mech. (1995), *vol.* 289, *pp.* 263–293

Sedimentation and entrainment in dense layers of suspended particles stirred by an oscillating grid

By HERBERT E. HUPPERT[1], J. STEWART TURNER[2] AND MARK A. HALLWORTH[1]

[1] Institute of Theoretical Geophysics, Department of Applied Mathematics and Theoretical Physics, University of Cambridge, 20 Silver Street, Cambridge CB3 9EW, UK

[2] Research School of Earth Sciences, Australian National University, Canberra ACT 0200, Australia

(Received 11 February 1994 and in revised form 7 November 1994)

Many flows, including those containing suspended particles, are kept turbulent by the action of the bottom stress, and this turbulence is also responsible for maintaining sedimenting particles in suspension and in some cases entraining more particles from the bed. A convenient one-dimensional analogue of these processes is provided by laboratory experiments conducted in a mixing box, where a characterizable turbulence is generated by the vertical oscillation of a horizontal grid. In the present paper we report the results of a series of experiments with a grid located close to the bottom boundary to simulate the action of stresses acting at a rough boundary, and compare the results with those obtained using the more extensively studied geometry in which a similar grid is located in the interior of a stirred fluid layer. Experiments have been conducted both with dense, particle-free fluid layers and with layers containing sufficiently high concentrations of dense particles to have a significant effect on the bulk density. In the fluid case, the interface at the top of the stirred dense layer continues to rise as lighter fluid is entrained across the interface. Sediment layers are distinctly different, because the particles responsible for the density difference between the layers can fall out of the suspension as it changes in thickness. The work done in keeping particles in suspension and the effect of this on the turbulence above the grid must be taken into account. The mechanism of resuspension of particles depends on the level of turbulence near the bottom boundary, below the grid. As the stirring rate, and thus the intensity of turbulence, are increased three possible equilibrium states can be attained sequentially: the particles eventually all precipitate; or some particles precipitate while the remainder are held indefinitely in suspension; or all the particles are suspended. In the last two cases a stable, self-limited suspension layer is produced, separated from the overlying fluid by a sharp density interface at a fixed height. Theoretical arguments are presented which provide a satisfactory scaling of the experimental data. These are compared with previous theories and numerical experiments aimed at modelling both the one-dimensional problem and the corresponding processes in turbulent gravity currents. Comparisons are also made with sediment-laden channel flows and convecting layers containing sedimenting particles. Similar results will hold for light, positively buoyant particles or non-coalescing bubbles.

1. Introduction

Turbulent layers of dense fluid, separated by a sharp interface from a less dense overlying fluid, occur in many natural contexts. In gravity currents, the lower layer flows under gravity down a slope or as a horizontal intrusion, and when the Reynolds number is sufficiently high, turbulence is produced and sustained by shear stresses acting at either the bottom or the interface. In one class of gravity currents the driving density difference may be due to either thermal or compositional effects. Examples include katabatic winds in the atmosphere or thermal fronts in the oceans and in lakes, and the laboratory analogues of these flows using a solute such as salt or sugar.

Another important class of gravity currents comprises flows in which the bulk density differences are due to the suspension of dense particles. These include fine silt in river outflows into the sea, sand in turbidity currents, ash in pyroclastic flows down the slopes of volcanoes, snow crystals in avalanches and phenocrysts in convecting magmas. A fundamental difference from gravity currents driven by purely compositional variations is that particles may settle out of sediment-laden flows, or be picked up from the bottom, so that the downslope buoyancy flux is not necessarily constant but may change with time and position downstream. The new set of questions posed by such flows includes the following. What determines the relative rates of settling and resuspension? Is it possible to achieve a steady state in which the two processes are in balance? Is the sharp top of a turbidity current dynamically the same as the entraining outer edge of a dense-fluid gravity current? These questions have been addressed previously in the sedimentology literature in various ways, but in the present work we have adopted a more fundamental approach.

A technique which has been extensively used to study turbulent mixing in stratified flows is to concentrate on the one-dimensional problem of mixing across an interface, which is simpler to set up and measure than a flow along a slope. In natural situations turbulence may be produced either mechanically or convectively, but here we consider only mechanical generation. A two-layer or continuous stratification is set up and stirred mechanically using a horizontal grid of solid bars, oscillated vertically. In most previous experiments the grid has been located in the interior of the fluid, well away from solid boundaries. A well-mixed turbulent layer forms, bounded by one or more density interfaces which propagate away from the oscillating grid as fluid is entrained into the stirred layer. The rate of propagation depends on the interfacial density difference and on the intensity of the turbulence near the interface, which is decaying with distance from the grid. The results obtained in this geometry are now reasonably well understood, as described in recent reviews by Turner (1986) and Fernando (1991).

In order to model the effects of the bottom stress in producing turbulence under a gravity current, we modified this convenient one-dimensional geometry by lowering the grid in a standard mixing box to a position much closer to the bottom. The dimensions of the box and the grid were kept the same (as detailed in the following section) so that direct comparisons could be made with previous results. A brief outline of the new experiments and the results in this geometry have been given by Huppert, Turner & Hallworth (1993). In the present paper we characterize this new configuration by making a more detailed comparison between the experimental results for the two geometries, using solute to provide the density difference. We then use this characterization to contrast the results of basal grid-stirring experiments using sugar solutions with those where a suspension of particles provides the density difference. The last case is of particular interest here, and the questions posed above for turbidity currents are translated into the following for stirred layers. Can the turbulent motions

keep the particles indefinitely in suspension, and under what conditions? Are there conditions under which only some of the particles can be maintained in suspension? What is the resulting depth of the suspension layer, and what are the dynamical conditions at its top?

In §2 below we first summarize the earlier grid-stirring results. We then present the new experiments with the grid close to the lower boundary and make a careful comparison between the two geometries. In §3 we discuss experiments in which the density increase in the lower layer is due to a suspension of small dense particles. The various possible time histories of experiments started with the same layer depth but different stirring frequencies are described briefly. We then concentrate on the steady-state conditions, first with layers of fully suspended particles and then layers in which only a fraction of the particles remain in suspension. The criterion for resuspension is also discussed at this point. In §4 a theory giving the layer depth in terms of the other observed parameters is presented, and effects at the top of the sediment layers are contrasted with those at the entraining fluid interfaces described in §2. The bottom boundary conditions, and the criteria for re-entrainment of particles from the bottom, are considered in §5. Comparisons are also made in §6 with theories and numerical experiments describing particle-laden flows in which either convection or a boundary stress produces the turbulence. The results are summarized in the final section, where the applications to the practical problems which motivated the research are also discussed.

2. Mixing across fluid density interfaces

2.1. *Summary of previous results with the grid in the interior of the stirred layer*

To set the scene for the new experimental results we first describe the mixing experiments previously conducted with the oscillating grid located well away from boundaries. In this discussion we draw heavily on the reviews by Turner (1986) and Fernando (1991). The paper by E & Hopfinger (1986) is also very helpful.

It became clear from the evaluation of the earliest experiments of this kind as described in particular by Turner (1968) and Thompson & Turner (1975) that the properties of the turbulence generated by a vertically oscillated grid depend strongly on both the geometry of the grid and on the amplitude of the oscillation. In later experiments therefore it has become customary to standardize the grid to a planar form and to use bars with a square cross-section and a spacing in the two perpendicular directions of $M/m = 5$, where M is the centre-to-centre spacing and m is the bar size. Most experiments have in fact been carried out in a standard square tank 254 mm × 254 mm × 450 mm deep using a grid having $m = 10$ mm and $M = 50$ mm, with five bars in each direction and half a grid space plus a small clearance at each end, rather than a solid bar along the walls. Some experiments, for instance those by Hopfinger & Toly (1976), have been conducted using a tank and grid with double these dimensions.

The mixing rate across the density interface bounding a dense stirred layer below a less dense layer at rest depends on a balance between inertia forces exerted by the turbulence and the restoring buoyancy forces in the close neighbourhood of the interface. Dimensional arguments show that the rate of entrainment v_E can be put in the form

$$v_E = \mathrm{d}z/\mathrm{d}t = v_1 f(Ri), \tag{1}$$

where f is a function of the Richardson number $Ri = g'l/v_1^2$, which is the ratio of buoyancy to inertia forces. Here $g' = g\Delta\rho/\rho_0$ is the reduced acceleration due to gravity,

where $\Delta\rho$ is the density difference across the interface and ρ_0 is the density of the upper layer, l is the integral lengthscale of the turbulence and v_1 is the r.m.s. value of the vertical component of the turbulent velocity, both measured in a homogeneous fluid at the same depth as the interface. It is important that these length and velocity scales are those appropriate for the turbulence which is actually doing the mixing. They can, however, often be related to overall parameters such as the layer depth and the velocity of the stirrer in particular geometries, as described below.

Hopfinger & Toly (1976) suggested that the available experimental results with square grids having $M/m = 5$ could be fitted by the expression

$$v_1/\omega S = CS^{1/2}M^{1/2}z^{-1}, \tag{2}$$

where ω is the frequency of oscillation and S is the stroke (twice the amplitude), and C is a constant which is about 0.30. The two most important features of this result are the linear dependence of velocity on stirring frequency and the decay of the r.m.s. velocity inversely with distance from the grid midplane. The integral lengthscale l increases linearly with distance from the grid, with a constant of proportionality of about 0.10 when S/M is less than 0.2, so that the product $v_1 l$ and the Reynolds number of the turbulence stay constant as it decays away from the grid. Using these relations to evaluate the scales near the interface, we may express the entrainment relation (1) as

$$v_E/v_1 = C_2 Ri^{-\beta}, \tag{3}$$

where $\beta = 3/2$. (C_2 is used here, and C_1 later in (4), to conform to the notation introduced by Huppert *et al.* 1993.) This power-law dependence in the limit where entrainment is controlled by non-diffusive processes (as it is in the experiments of interest here which use solutes such as sugar and salt to produce the density differences) has been confirmed by the later measurements of E & Hopfinger (1986), which also support the previously suggested frequency dependence.

As more measurements have been reported in the literature, however, the picture has become more complicated rather than being clarified. Fernando's (1991) review has shown how subtle changes in the experimental configuration can affect the results and their interpretation, and the value of the power β in (3) is still the subject of controversy. There are several sets of careful experiments which support a value of β closer to 1.2 for the salt-stratified case, and arguments have been put forward that suggest that the higher values may be due to the use of inappropriate velocity or length scales. Nokes (1988) deduced that for his experiments covering a range of strokes up to 3.2 cm, the decay law is more nearly $z^{-1.5}$. This range includes that used in the present experiments. In deducing the value $\beta = 1.2$ from his data, however, Nokes avoided the necessity of using any explicit decay law by calculating the entrainment rates for different stirring rates at fixed distances from the grid. There is also a theoretical argument by Long (1978) leading to the prediction (Fernando 1988) that $\beta = 7/4$, but there is little experimental support for a value as high as this.

Certainly the particular form (2) chosen for the decay of velocity with distance away from the grid affects the power which is deduced in (3), and in our interpretation of the new experiments we will use the more general, dimensionally correct expression

$$v_1 = C_1 \omega d^{\alpha+1} z^{-\alpha}. \tag{4}$$

That is, we allow for a general power-law decay rate and introduce a representative lengthscale d which incorporates all the other lengths specified by the geometry of the grid and its stroke. This descriptive lengthscale was kept constant over the series of experiments. Both α and β will be deduced from the measurements, making no prior assumptions about either.

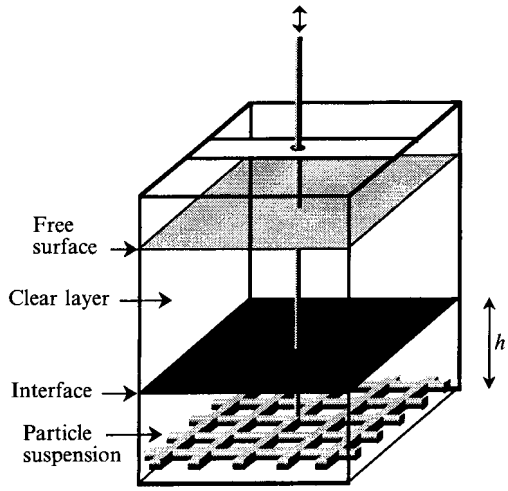

FIGURE 1. Sketch of the stirring box geometry used in the experiments.

2.2. *Stirring with the grid near the bottom boundary*

The geometry used in all the quantitative experiments reported below is sketched in figure 1. We lowered the grid of 10 mm square bars in the 'standard' mixing box to a mean height above the bottom, $\bar{z}$, of 19 mm, and oscillated it with an amplitude of 12.5 mm. At the extreme position in the downward oscillation there was therefore a clearance above the bottom of 1.5 mm.

The density differences in the experiments without particles were produced by dissolving sugar in the lower layer. All experiments began with a 60 mm deep layer of sugar solution below a 220 mm layer of fresh water. Seventeen experiments were conducted covering different combinations of grid-oscillation frequencies ω and initial density differences $\Delta\rho_0$. In each run the depth of the lower layer was recorded as a function of time t as it deepened due to the entrainment of upper layer fluid. Once the depth exceeded 80 mm both the near-grid effects and the difference between the layer depth h and the distance z ($= h-\bar{z}$) between the mean position of the grid and the interface became unimportant, and as shown in figure 2 the observations were well fitted by a power-law relationship of the form

$$z = Bt^b, \tag{5}$$

where B is a function of ω and $\Delta\rho_0$ and the mean value of b, $\bar{b} = 0.151 \pm 0.008$, is independent of these two parameters.

In the Richardson number which is defined following equation (1), the reduced gravity g' is decreasing as the layer deepens but $g'h$ is constant, by the conservation of solute. Since $g'h$ is to a good approximation equal to $g'z$, and l is proportional to z, $g'l$ can also be taken as constant. Thus in each individual run, Ri changes with time only because v_1, the turbulent velocity near the interface, is varying with distance from the grid.

Substituting the general power-law expressions (3) and (4) into (1), and integrating to express z as a function of t, we obtain

$$z = C_3(g'h)^{-\beta/[\alpha(2\beta+1)+1]}\,\omega^{(2\beta+1)/[\alpha(2\beta+1)+1]}t^{1/[\alpha(2\beta+1)+1]}, \tag{6}$$

where C_3 is a constant which incorporates the previous constants. Note that we have retained the directly measurable h in this relation, rather than using the deduced l

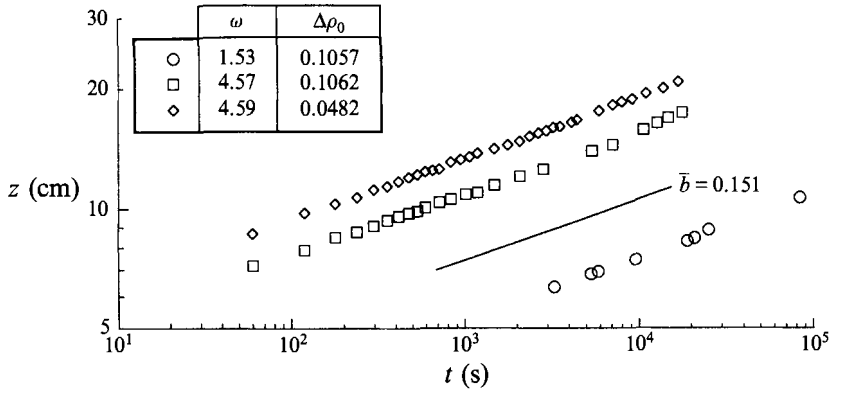

FIGURE 2. The results of three typical experiments with a stirred layer of sugar solution entraining fresh water from above for different values of ω and $\Delta\rho_0$. The layer depth is plotted as a function of time on logarithmic scales in the form suggested by equation (5) together with a line of slope 0.151. This average slope for all the experiments is included for comparison.

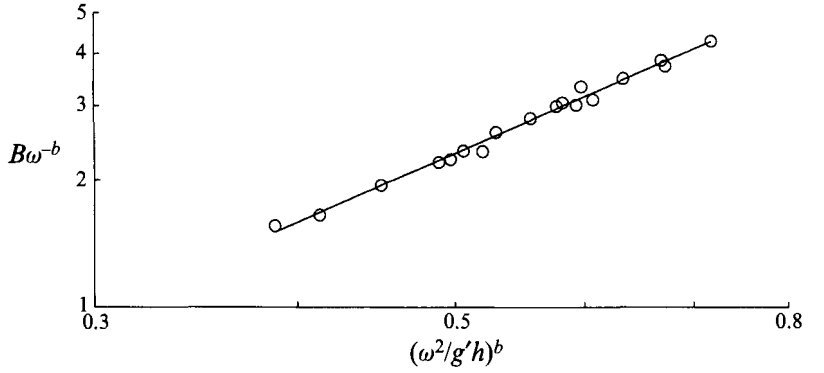

FIGURE 3. Comparison between the experimentally determined values of B from figure 2 and the corresponding factor in equation (6). Plotting $B\omega^{-b}$ against $(\omega^2/g'h)^b$ allows both α and β to be evaluated using the line of best fit, as described in the text.

which is proportional to h. Comparing (6) with (5) we see that $\alpha(2\beta+1)+1 = b^{-1} = 6.62\pm0.35$.

Another relationship linking α and β can be obtained by comparing the experimentally determined values of B with the corresponding time-independent factor in (6). This is conveniently done by plotting $B\omega^{-b}$ against $(\omega^2/g'h)^b$ for all the experiments on a log–log plot as shown in figure 3. The slope of the best-fit straight line gives directly $\beta = 1.696\pm0.072$ and hence, using the previous relation, $\alpha = 1.28\pm0.11$.

2.3. *Comparison between the two sets of experiments*

Very few experiments have previously been conducted in which the distance of the grid from the bottom boundary has been systematically varied. Nokes (1988) reported a few runs of this kind, but in no case was the grid as close to the boundary as in the present experiments. Nokes showed that moving the grid closer to the boundary increased the intensity of the turbulent motions above the grid, presumably because of the reflection of some of the energy propagating downwards, but the rate of decay remained unchanged under the stirring conditions he used.

For the present experiments with the grid close to the boundary, there is a substantial difference in behaviour in comparison with the interior stirring experiments.

The decay rate for velocity, with the grid close to the bottom, described by $\alpha = 1.28$, lies between the commonly adopted value 1.0 and that deduced by Nokes for his series of measurements at fixed distances from the grid, namely $\alpha = 1.5$. But the dependence on Richardson number, with $\beta = 1.7$ rather than the value 1.2 deduced by Nokes (or 1.5 if the earlier internal mixing results are given more weight), is definitely stronger with the grid close to the bottom. It is in fact close to the value proposed by Long (1978).

The important point for the present purposes is that we have quantified the influence of the oscillating grid on entrainment across a receding interface directly in the new geometry. This same geometry has been used in the experiments with sediment layers, so that it will be appropriate to make some direct comparisons between the two sets of experiments. It would not have been valid to assume that the previously published results in stirring boxes would be applicable to the situation of interest here.

3. The maintenance of suspensions by grid stirring

We now present the results of experiments in which the density increase in the lower layer was due to a suspension of silicon carbide grit, which has a density ρ_p of 3.217 g cm^{-3}. Different size grades of the irregularly shaped silicon carbide particles were used (see figure 1 of Huppert *et al.* 1991 for micrographs of two of the grades), with effective median diameters λ of 5.5, 5.8, 10.8, and 17.6 μm, where the effective diameter is the diameter of a spherical particle with the same settling velocity at low Reynolds number (the Stokes free fall velocity v_s). A measured mass M_0 of particles suspended in water was added rapidly under a layer of fresh water, using a pipe extending to within a few millimetres of the bottom of the experimental tank. The grid was then oscillated with frequency ω, and the system allowed to come to equilibrium. The frequency was then reduced in steps, and the properties of the new final states measured each time. All the quantitative experiments were conducted using the standard stirring box and grid described above.

3.1. *The time history of suspension layers*

The time histories of the layer depth and the particle concentrations were not monitored in detail during the main series of experiments. We first conducted some preliminary experiments using a smaller box and a (non-standard) grid made of flat metal strips. It is instructive first to present some data obtained in these qualitative experiments before we present our detailed quantitative results from the main series of experiments. We note first that the time history of the layer depth and the particle concentrations are distinctly different from that of the experiments with sugar solution in the lower layer, since the particles can migrate through and fall out of the stirred layer as it changes in thickness, rather than just contributing to the bulk density difference.

In particular, instead of continuously deepening (as described by (5) for entraining fluid layers), the layer behaviour changes greatly as ω and hence the intensity of turbulence is increased, even when the particle size and initial concentration are held fixed. This is illustrated in figure 4 using data for three different stirring frequencies, with the same depth and concentration of particles in the lower layer. At the lowest stirring rate the particles eventually all precipitate while the layer depth first decreases (producing a transient increase in particle concentration), and then increases without limit. For an intermediate level of turbulence (with $\omega = 1.67$ Hz) some particles remain in suspension after a long time, and the layer depth goes through a minimum before

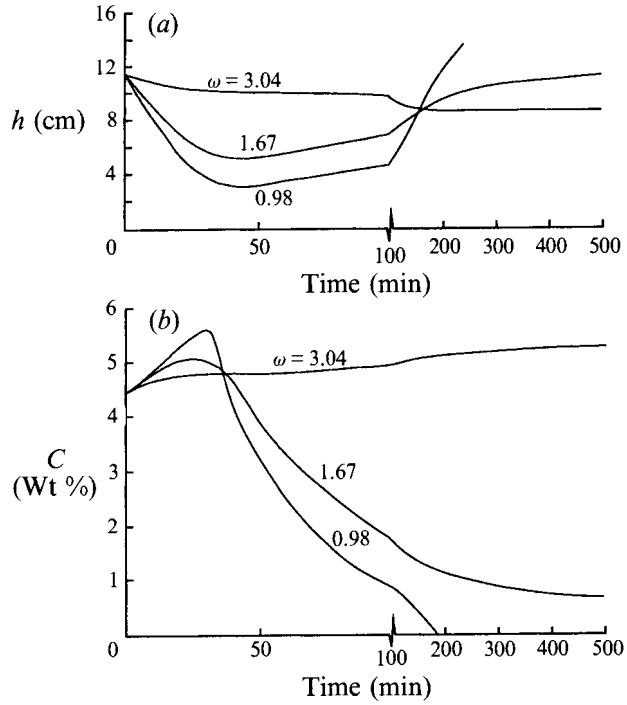

FIGURE 4. The evolution of (*a*) the layer depth and (*b*) the concentration C of suspended particles for three different stirring frequencies ω in a single experiment.

λ (μm)	5.5	5.8	10.8	17.6
ω_1 (Hz)	0.75	0.9	1.0	1.2
ω_2 (Hz)	2.6	2.7	3.4	4.0

TABLE 1. Effective particle diameters, and the two critical stirring frequencies introduced in the text.

reaching an asymptotic steady depth close to the initial value. With still higher stirring frequencies, all the particles are held in suspension in a layer which is slightly shallower and more concentrated than the initial distribution. An explanation of these different behaviours in the steady state will be given in the following sections. These results are clearly preliminary, and it will be interesting to pursue these transient experiments more thoroughly in the future.

3.2. *Steady-state suspension layers*

We concentrate now on the measurements of the final layer properties in the experiments using the standard stirring box and grid geometry where a steady state was attained. As seen from figure 4 the approach to this steady state often took several hours. For a given particle size, two critical frequencies could be identified, as summarized in table 1. Below a critical frequency ω_1 (dependent only on the size of particles, and not on the initial mass of particles M_0) the intensity of turbulent stirring was insufficient to maintain any of the particles indefinitely in suspension, and eventually they all fell to the floor. (The factors determining the equilibrium conditions at the bottom boundary will be discussed in more detail in §5.)

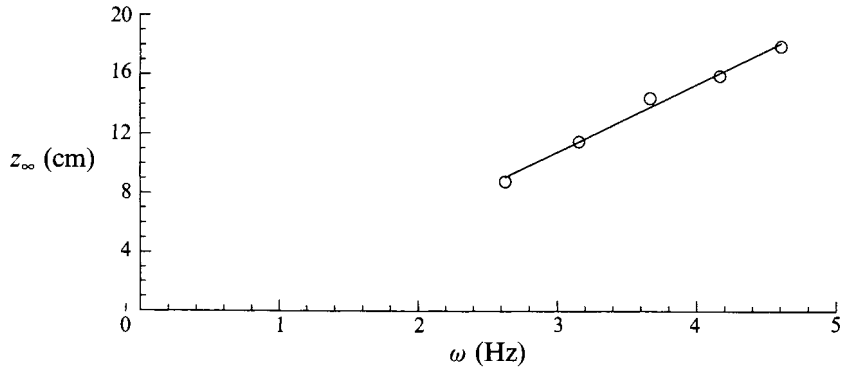

FIGURE 5. The final depth z_∞ of a sediment layer as a function of stirring frequency ω for an individual run in which all the particles of diameter 5.5 μm were held in suspension ($M_\infty = M_0 = 177$ g and $\omega > \omega_2$).

Above a second critical frequency ω_2 all the particles could be held in suspension. For small M_0 the depth of the sediment layer continued to increase up to the free surface, but for sufficiently large M_0 the suspension layer thickness reached a final steady value $h_\infty (= z_\infty + \bar{z})$, which is a function of frequency ω (and also the size of the particles) but independent of the initial thickness of the layer containing the particles. In this regime the total mass of particles in suspension was constant, and z_∞ is approximately linearly proportional to ω, as shown for an individual run in figure 5. The constant of proportionality is dependent on the total mass $M_0 = M_\infty$, and the final concentration C_∞ of particles in the suspension, assumed to be constant with depth, is equal to the final mass M_∞ divided by the final volume of the suspension layer.

At frequencies between ω_1 and ω_2 some of the particles fell to the floor while a fraction remained suspended in a layer, the final thickness of which was again independent of the initial thickness. It was found that the final depth z_∞ was again a function of ω, the particle size and M_∞ only, so that once the mass remaining in suspension is known it is not necessary to specify whether all or only a fraction of the particles remained in suspension. Figures 6 and 7 present all the quantitative measurements of the final depth of the suspension layer above the grid $z_\infty (= h_\infty - \bar{z})$, for the whole of the frequency range covered†. (The theory developed in §4 below indicates that instead of z_∞ we should use $z_\infty (z_\infty / h_\infty)^{1/3}$ in the ordinates of these figures, but the difference between z_∞ and h_∞ is so small for most of the data that the plots are changed very little.)

Figure 6 is a plot of z_∞/ω versus M_∞, for different sized particles on logarithmic scales. In each case M_∞ was determined by withdrawing a sample from the centre of the suspension layer, allowing it to settle, and weighing before and after decanting and drying to deduce the liquid and solid fractions, and hence C_∞ and M_∞. The stirring frequency was lowered in steps, and the system allowed to come to equilibrium each time before measuring the new values of z_∞ and M_∞. In many experiments the size distributions of the particles sedimented on the bottom of the tank and those remaining in suspension were measured and compared. The distributions were not detectably different, showing that differential settling, with the larger particles falling out first as ω is decreased, is not responsible for the variation of M_∞ with ω. It seems likely that with a broader distribution of particle sizes differential settling could be a significant

† A detailed listing of all the runs and the quantitative results is available from the JFM Editorial office.

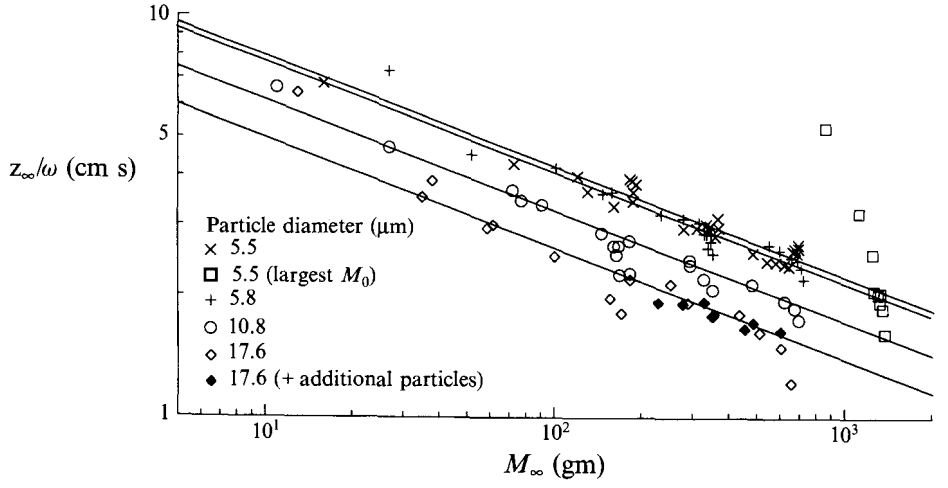

FIGURE 6. Plot of z_∞/ω versus M_∞ on logarithmic scales for different sized particles and a wide range of stirring frequencies. The best-fit lines to the form $z_\infty M_\infty^\mu \propto \omega$ have a slope μ of -0.275, and the constant of proportionality is a function of the particle diameter.

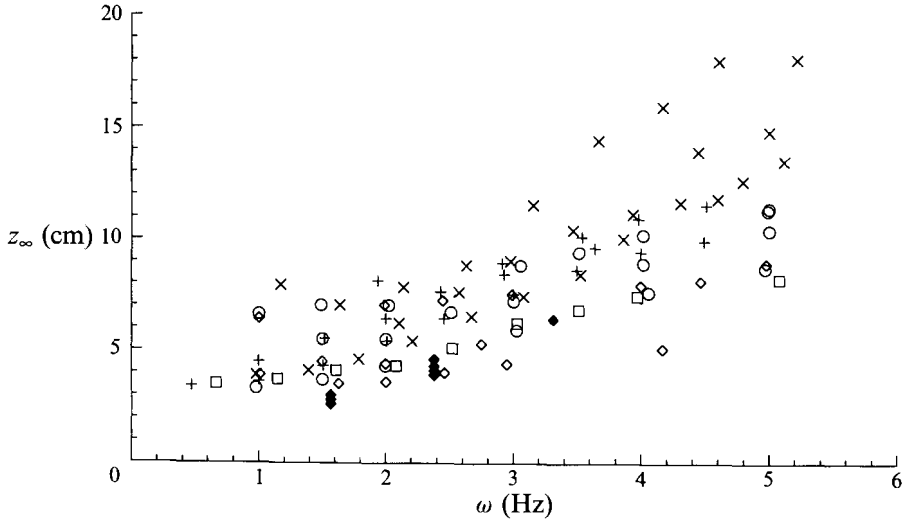

FIGURE 7. Plot of z_∞ versus ω for all the experimental runs with various particle sizes and masses in suspension. Compare this with figure 8, in which the data are scaled in accordance with the theory presented in §4. Symbols as figure 6.

factor, but this lies outside the scope of the present experiments and paper. The important dynamic effect of variations in particle size is expressed in the Stokes free fall speed v_s, for a particle of diameter λ, which is given by

$$v_s = g(\rho_p - \rho_a)\lambda^2/18\rho_0\nu, \tag{7}$$

where ρ_a is the density of the ambient fluid and ν its kinematic viscosity. The values of v_s corresponding to the median particle sizes will be used in the comparisons with the following theory. Any effects which might be due to hindered settling are not incorporated.

The lines fitted to the data for each particle size in figure 6 show that there is good consistency over the range $\omega_1 < \omega < \omega_2$, with $z_\infty M_\infty^\mu \propto \omega$, where the constant of

proportionality is a function of the particle diameter λ and perhaps some other geometrical factors. The best-fit lines for all the particle sizes used have a slope μ of -0.275 on this plot. However, in the experiments with the largest values of M_0, when nearly all the particles were in suspension, the measured values of z_∞/ω fall below these lines. Under these conditions there is virtually no change in M_∞ (since it cannot increase above M_0) and the final depths of the layers decreased slightly for a given ω. These, and the anomalous results on the right of figure 6 (plotted as the open squares), will be considered further in § 5 in the context of our discussion of the bottom boundary conditions.

The linear plot of z_∞ versus ω, with the experimental data collected together in figure 7 for all particle sizes and masses in suspension, does not show the dependence on M_∞ and particle size (or v_s) and there is a great deal of scatter. It is given here for later comparison with the same data scaled in accordance with the theory developed in § 4.

4. Theoretical interpretation of the experimental results

4.1. *Comparison between dense fluid layers and suspensions*

In seeking to explain the data presented above, and to scale the measurements to bring data from different runs into a common form, we have considered several alternative ideas. The first has been foreshadowed in § 2: can the entrainment relation (1) obtained for dense fluid layers, with the powers α and β in equations (3) and (4) evaluated in experiments with the grid close to the bottom boundary, be carried across to suspensions? The extra hypothesis required in the latter case is that the sediment layer stops growing when the particle fall velocity v_s just equals the entrainment velocity v_E.

This can be tested as follows. Substituting (3) and (4) into (1), we obtain

$$v_E = kC_4^{-\beta}\omega^{2\beta+1}z^{-\alpha(2\beta+1)}, \tag{8}$$

where k incorporates the constants C_1, C_2 and d, and $g'h = C_4$, which is a constant (independent of time) for each fluid layer experiment (by conservation of mass). For the steady state of the corresponding experiment with particles we can assume that $C_4 \propto M_\infty$ when $z = z_\infty$. Replacing v_E by v_s in (8) and rearranging, we obtain

$$z \propto \omega^{1/\alpha} M_\infty^{-\beta/\alpha(2\beta+1)}\, v_s^{-1/\alpha(2\beta+1)} \tag{9a}$$

and inserting the numerical values $\alpha = 1.28$ and $\beta = 1.70$ yields

$$z_\infty \propto \omega^{0.78} M_\infty^{-0.302}\, v_s^{-0.178}. \tag{9b}$$

This power-law dependence of z_∞ on ω is not borne out by the experiments. When $z_\infty/\omega^{0.78}$ is plotted against M_∞, no ordering of the data is achieved, whereas figures 5 and 6 give strong support to the conclusions that z_∞ is proportional to ω. Further, if v_E is calculated using (8) for all the final layer depths measured in experiments with a given particle size, there is a wide variation. Thus the entrainment velocity cannot be balanced by particles falling away from the interface with a fixed settling velocity.

4.2. *Fluid layers with an imposed buoyancy flux*

A more productive approach is to draw an analogy between sediment layers and fluid layers which have a stabilizing buoyancy flux superimposed on mechanical stirring. The classic example of this situation is wind blowing over the heated surface of the ocean, producing turbulence which mixes the heat downwards to a depth

$$D = au_*^3/B, \tag{10}$$

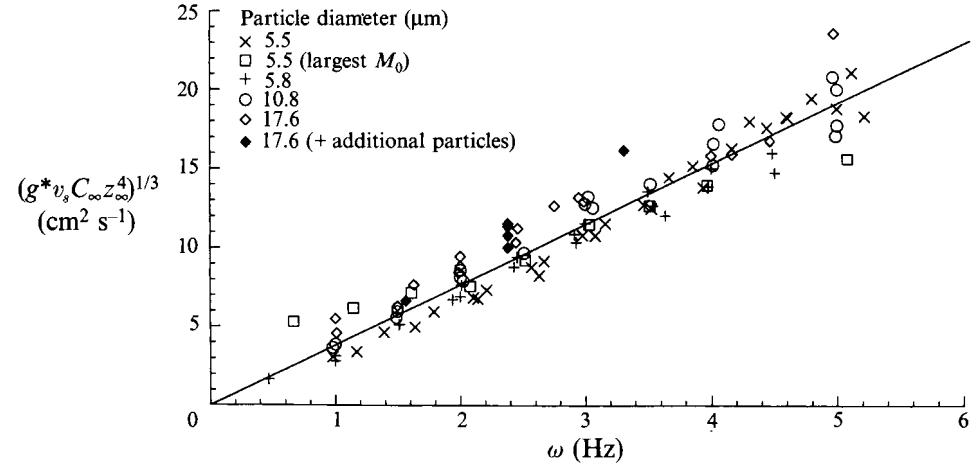

FIGURE 8. All the experimental data scaled using the theory leading to equation (19). There is a very satisfactory collapse of the data for all particle sizes onto a straight line with slope 3.85. (Compare with the unscaled plot, figure 7.)

where u_* is the friction velocity, B is the buoyancy flux and a is a constant. This form was first suggested by Kitaigorodskii (1960) on dimensional grounds. The depth D is in fact proportional to the Monin–Oboukhov length, and (10) implies that a constant fraction of the kinetic energy input is being used to change the density of the mixed layer. The density of the surface layer decreases (as the temperature increases) linearly with time, while D stays fixed. There is thus *no* entrainment across the edge of the well-mixed layer; all the turbulent kinetic energy is being used to change the potential energy of the layer, and the turbulent velocity falls to zero at the interface. This same model will also be relevant for the (inverted) case of a turbidity current picking up sediment, where the turbulence generated by the bottom stress is providing energy to lift the entrained dense particles.

When grid stirring replaces the surface stress as the source of the turbulence, Hopfinger & Linden (1982) have shown that (10) no longer gives a satisfactory description of the equilibrium layer depth. Instead, a local energy balance must be used, in which the viscous decay of the turbulence away from the stirring grid is taken into account, i.e. the decay of velocity according to (4) must be incorporated into the theory, as well as the effect of the buoyancy flux. In order to lay a foundation for our subsequent discussion, the results of Hopfinger & Linden's (1982) analysis for grid-stirred fluid layers will now be summarized, with a critical assessment of the assumptions they have incorporated. We then discuss the extension of their model to layers of suspended particles and (in a later section) its relation to numerical models of the suspension mechanism.

In a homogeneous fluid, the turbulent kinetic energy equation for a spatially decaying turbulent velocity u can be written as

$$r\,\mathrm{d}u^3/\mathrm{d}z = -u^3/qz, \tag{11a}$$

where r is a constant (found experimentally in fluids of constant density to be given by $r = 2.2$) and the integral lengthscale $l = qz$. This linear increase of l with distance from an origin near the grid centreline has been assumed in virtually all theories, including those presented in §2. The solution of (11a) is

$$u = u_0(z/z_0)^{-1/3rq}, \tag{11b}$$

where u_0 is the velocity at z_0 some distance from the origin. Hopfinger & Linden (1982) adopted $\alpha = 1$ in the notation of equation (4), the value proposed by Hopfinger & Toly (1976) for grid stirring in the centre of a layer. In the following analysis we will use $\alpha = 1.28$ as determined by our new measurements with the grid near the boundary and modify Hopfinger & Linden's argument accordingly. This implies that $rq = 0.26$ (instead of the previously adopted value of 1/3). To simplify the resulting equations the notation $(rq)^{-1} = \theta$ will also be introduced in (14) below, with the value $\theta = 3.84$ corresponding to the new geometry.

When a buoyancy flux is imposed near the level of the stirring grid, another term must be added to the right-hand side of (11*a*) and it becomes

$$r\,\mathrm{d}(u^3)/\mathrm{d}z = -u^3/qz + (g/\rho_0)\overline{w'\rho'}, \tag{12}$$

where w' and ρ' are the fluctuating velocity and density. If we suppose that the density is independent of height and that the layer remains well mixed as its density changes, then the buoyancy flux is a linear function of height and must fall to zero at the edge of the layer. Hence

$$(g/\rho_0)\overline{w'\rho'} = B_0(z-D)/D, \tag{13}$$

where B_0 is the buoyancy flux at the origin. We substitute (13) into (12) and solve for u, with the boundary condition $u = u_0$ at $z = z_0$. The solution in dimensionless form is, for distances from the grid such that $(z/z_0)^4 \gg 1$,

$$\left(\frac{u}{u_0}\right)^3 = \left(\frac{z}{z_0}\right)^{-\theta}\left\{1 - \frac{1}{r}\left(\frac{z}{z_0}\right)^{\theta}\frac{B_0}{Du_0^3}\left[\frac{Dz}{1+\theta} - \frac{z^2}{2+\theta}\right]\right\}. \tag{14}$$

Making the further assumptions that the density gradient is sufficiently weak for θ to have the same value ($\theta = 3.8$) as for the case without a buoyancy flux *but with the grid near the bottom boundary*, (14) becomes in dimensionless form

$$\left(\frac{u}{u_0}\right)^3 = \left(\frac{z}{z_0}\right)^{-3.8}\left\{1 - \frac{1}{r}\left(\frac{z_0}{D}\right)\left(\frac{z}{z_0}\right)^{4.8}\left(\frac{B_0 z_0}{u_0^3}\right)\left[\frac{D/z_0}{4.8} - \frac{z/z_0}{5.8}\right]\right\}. \tag{15}$$

Mixing stops at the top of the mixed layer, and (15) shows that $u = 0$ when $z = D$, if

$$\frac{D}{z_0} = (28.3r)^{0.21}\left(\frac{u_0^3}{B_0 z_0}\right)^{0.21}. \tag{16}$$

Thus it is predicted that the mixed-layer depth scales with $(u_0^3/B_0)^{0.21}$ for fixed z_0 rather than having the form (10) suggested by the Monin–Oboukhov scaling. The power is a consequence of the measured decay law for turbulent velocity adopted here; the original calculation by Hopfinger & Linden (1982) used a 1/4 power corresponding to $\alpha = 1$. They also compared this with the power $2/11 = 0.182$ resulting from the use of $\alpha = 1.5$, and their experimental data gave some support to both these forms for different ranges of the layer depth.

It is instructive to plot out some of the above results so that the effect of the buoyancy flux on the turbulence under these assumptions can be appreciated more fully, but this will be deferred to §5; they will also be compared with numerical treatments of this problem in §6. We first proceed with the application of these ideas to the explanation of our measurements of the equilibrium depth of layers of sedimenting particles.

4.3. *Extension of buoyancy flux model to suspensions of particles*

E & Hopfinger (1987) have shown how a further simple and physically plausible assumption allows (15) and (16) to be applied to layers of sedimenting particles stirred with an oscillating grid. They assumed that in equilibrium, when the mass of particles

in the layer is steady, the upward solid particle flux due to the turbulent transport must be equal and opposite to the downward flux due to particle settling. Work must be done on the particles to keep them in suspension, and this is equivalent to a stabilizing buoyancy flux which can be related to the settling rate. Because the two transports are equal and opposite, the density of the suspension remains constant and nearly uniform with depth. This will not be quite correct at the top of the layer, where some settling must occur, and the fall-velocity distribution might enter the problem. (In addition, in very concentrated sediments the gradient of concentration may become important, as discussed further in §5.)

Explicitly, the stabilizing buoyancy flux equivalent to $(g/\rho_0)(\overline{w'\rho'})$ in (13) is now

$$(g/\rho_0)\,\overline{w'\rho'} = (g^* v_s C)(z-D)/D, \tag{17}$$

where $g^* = g(\rho_p - \rho_a)/\rho_a$, ρ_p being the density of the solid particles and ρ_a the fluid density, v_s the settling velocity and C the (dimensionless) volume concentration of particles. The further development of the theory then follows the arguments leading to (14) and (16), with B_0 replaced by the particle buoyancy flux $(g^* v_s C)$. E & Hopfinger (1987) used the decay law with $\alpha = 1$ and hence the power 1/4 in (16) and expressed the equilibrium suspension layer depth as

$$D = (20r)^{1/4}(u_0 z_0)^{3/4}(g^* v_s C)^{-1/4}. \tag{18}$$

The essence of E & Hopfinger's mechanistic theory is contained in the following dimensional argument. The fluid motions near the oscillating grid are described by a single parameter ωd^2, the 'grid action', where d is the representative length introduced in (4) and ω is the stirring frequency. In the notation used in (18) this is equivalent to $u_0 z_0$. The buoyancy flux associated with particles falling out (and being lifted and held in suspension) is $g^* v_s C$, as described above. If ωd^2 and $g^* v_s C$ are the only two physically relevant parameters on which the final depth above the grid depends, it follows on dimensional grounds that

$$z_\infty = (\omega d^2)^{3/4}(g^* v_s C_\infty)^{-1/4} \tag{19a}$$

or

$$(g^* v_s C_\infty z_\infty^4)^{1/3} = \omega d^2. \tag{19b}$$

It may be convenient to express this in terms of the total mass in suspension, M_∞, defined on the assumption that the concentration remains uniform right to the bottom of the tank. (Allowance could be made if necessary for the layer of sediment deposited on the bottom of the tank, but this refinement is not justified in the current context; it is discussed further in §5.) Using the relationship $M_\infty = A\rho_p h_\infty C_\infty$ between the load M_∞ of particles in suspension and the final volume concentration, where A is the cross-sectional area of the tank, and taking due account of the difference between z_∞ and $h_\infty (= z_\infty + \bar{z})$, (19) can be rewritten as

$$z_\infty = (\omega d^2)(g^* v_s M_\infty / A\rho_p)^{-1/3}(1 + \bar{z}/z_\infty)^{1/3}. \tag{20}$$

4.4. *Rescaling and discussion of the experimental results*

A plot of all the data collected in figure 7, scaled using (7) and (19*b*), is given in figure 8, where different symbols have been used for the four sizes of particles. There is a very satisfactory collapse of the data onto a straight line (with best fit $d = 19.6$ mm), which gives good support to the above theory. The major source of the scatter is, we believe, the distribution of particle sizes and the uncertainty in median particle size due to the possible disaggregation of particle clumps before the sedigraph measurements. The straight-line fit for individual particle sizes is much better than that obtained with a

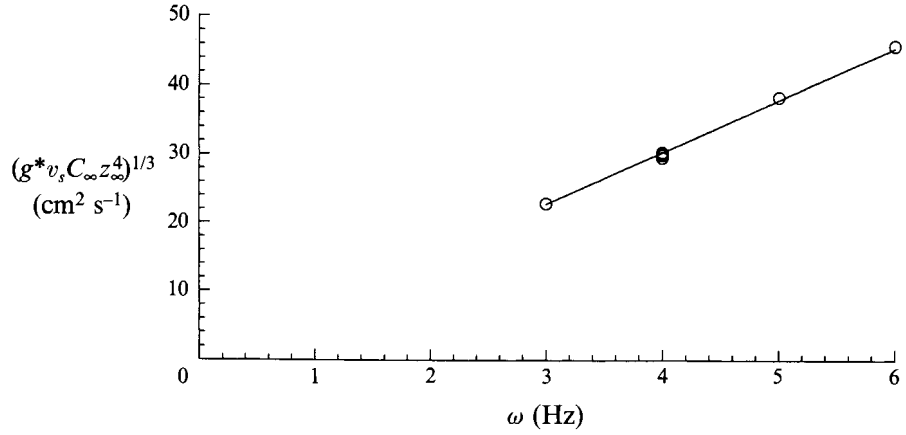

FIGURE 9. The data of E & Hopfinger (1987), scaled according to equation (19). Their experimental results using a different grid size and bottom boundary conditions are well fitted by the same form as our data shown in figure 8, but with a different constant of proportionality.

simple use of the (inappropriate) fluid layer entrainment relationship. The data of E & Hopfinger (1987), obtained using a larger grid of the same form but with a different bottom separation distance and stroke, are plotted in figure 9. They are well fitted by the same functional form, with a constant $d = 27$ mm.

5. The bottom boundary conditions

The experimental data presented above have shown that once the equilibrium load M_∞ of sediment held in suspension is specified, there is good support for our choice of the physically most significant parameters. That is, the sediment layer depth can be determined as a function of M_∞, the stirring frequency ω which specifies the intensity of turbulence in the region above the grid, and the particle fall velocity v_s which is related to the buoyancy flux due to the particles. Two questions require further discussion: how is M_∞ related to M_0 when only a fraction of the particles is held in suspension, and what determines the rate of 're-entrainment' of particles settling on the bottom? Both of these are related to the bottom boundary conditions, but it is desirable to distinguish between results that can be explained in terms of the properties of the turbulence decaying above the grid, as we have already done in the previous discussion, and those that require the consideration of the interaction between the turbulence below the grid and the layer of deposited particles.

5.1. *Energy argument for particle suspensions*

Consider first an experiment which was started with an initial load M_0, and has reached the stage where some particles have settled on the bottom of the tank. Suppose that the particles have been deposited because a given mechanical energy input into the turbulence close to but above the grid can support only a certain (maximum) particle concentration C_∞, associated with a maximum buoyancy flux. If ω and hence the energy input are increased, it follows from (20) that this general relationship is satisfied if there is an associated increase in M_∞, the mass of particles in suspension, with z_∞ changing little. For example, for a particular series of experiments we found that z_∞ remained approximately constant (within the experimental error) while M_∞ was proportional to ω^3.

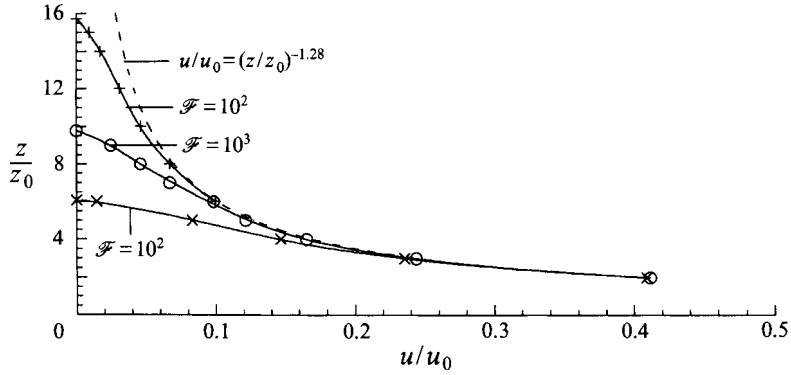

FIGURE 10. The turbulent velocity as a function of distance from a stirring grid, when there is a stabilizing buoyancy flux. The velocity has been calculated using equations (15) and (16) obtained from a modified form of the theory due to Hopfinger & Linden (1982). The decay rates for three values of the parameter $\mathscr{F} = (u_0^3/B_0 z_0)$ are compared with the behaviour when there is no buoyancy flux.

The results discussed above are similar to those obtained by E & Hopfinger (1987), which they explained in terms of an unnecessarily restrictive energy argument. The relations (19) and (20) imply that the sediment load is determined mainly by the properties of the turbulence near the grid, and the buoyancy flux through the layer immediately above it. It is instructive at this point to refer back to the argument leading to the relationship (16), the mixed-layer depth for fluid layers with a stabilizing buoyancy flux, which was extended to suspensions of particles. Whatever decay law is later used for the turbulent velocity, the dimensionless group $(u_0^3/B_0 z_0) = \mathscr{F}$ say, expresses the balance between the properties of the turbulence and the buoyancy flux near the grid. The above argument is equivalent to the statement that, when $\mathscr{F}$ is held constant (by varying B_0 and u_0, or M_∞ and ω, simultaneously) then $D = z_\infty$ also has a constant value.

The relation (15) can be used in conjunction with (16) to illustrate the effect of changes in $\mathscr{F}$ on the layer behaviour. Figure 10 shows the variation of turbulent velocity with distance from the grid calculated for three values of $\mathscr{F}$ and compared with the decay when there is no buoyancy flux. The buoyancy flux is decreasing linearly to zero at the top of the layer according to the model, and it begins to have a significant effect on the turbulent velocity (reducing it by 4%) at $z/z_0 \approx 3$ when $\mathscr{F} = 10^2$ and the corresponding $D/z_0 = 6.08$. For $\mathscr{F} = 10^3$, $D/z_0 = 9.78$ the same fractional reduction occurs at $z/z_0 \approx 5$, and for $\mathscr{F} = 10^4$, $D/z_0 = 15.74$ it occurs at $z/z_0 \approx 8$, approximately half the total depth in each case. This behaviour will be compared with the results of the numerical computations of Noh & Fernando (1991*a*, *b*), discussed in §6.

5.2. *Direct effects of the sediment layer on the bottom boundary*

When M_0 is increased beyond about 600 g (the upper limit of the range discussed in the previous section), the equilibrium value of z_∞ decreases for a given ω while M_∞ increases (as shown, for example, by the lowest points at the right of figure 6). This implies that more particles have been held in suspension because more are available. This behaviour is probably associated with the fact that the effective turbulent velocity acting on the particles near the bottom is increased when the settled layer of particles is deeper so that the effective layer depth beneath the grid is less. We need therefore to consider the detailed geometry of the sediment layer in relation to the grid, including

the shape of the cusps formed at the top of this layer, and the variation of the turbulent fluid velocities very close to it in the space between the mean position of the grid and the floor.

It is likely that a 'near field' velocity pattern occurs rather than the kind of power-law decay of velocity we have used to describe the turbulence above the grid. In some experiments with the larger values of M_0, the grid, if brought to rest at the bottom of its travel, would be buried in sediment if all the particles settled out. For example if 710 g of particles all settled out on the bottom in the absence of the grid, the depth of the sediment layer would be 7 mm. A small extra deposit of sediment would decrease the grid–sediment layer distance, and thus subject the sediment to a large increase in fluid velocity which would tend to resuspend it.

The above interpretation is supported by the results of experiments in which successive extra weights of sediment were added to the tank while stirring was continued at a fixed frequency (2.28 Hz). For example, starting with 355 g of particles in suspension, a steady state was attained with 230 g of particles left in suspension, and hence 125 g on the floor. Two further additions of 135 g of particles each were made and the suspension layer allowed to come to equilibrium at each stage. Each addition was accompanied by a corresponding decrease in z_∞ but no more particles sedimented during either period, so that the values of M_∞ and B_0 increased and the ratio $\mathscr{F} = (u_0^3/B_0 z_0)$ decreased. In each case, the values for the final mass in suspension as a function of ω and the other parameters were consistent with (20), so that the previously determined conditions above the grid are still relevant; the points corresponding to this experiment are marked as black diamonds on figure 8. However, the constancy of the weight (and thickness) of sedimented particles implies that the variation of the turbulent intensity near the bottom is extremely large over distances of a few mm, and suggests the following interpretation of the lower critical frequency ω_1 shown in table 1. For each stirring frequency the level of turbulence in the region below the grid allows a critical amount of sediment M_* to settle, until the deposited layer reaches a certain depth, which depends on ω. At sufficiently low ω, depending on the particle size, all the particles can settle and not be re-entrained, because nowhere on the bottom boundary are the velocities produced by the grid large enough to resuspend the particles.

With the largest values of M_0 and the smallest particles used in our experiments the relationship between z_∞/ω and M_∞ changed dramatically, as shown by the open squares on the right-hand side of figure 6. The final depths of the suspension layers were small and the concentrations very high. It seems probable that the turbulent velocities were in the 'near field' regime both below and above the grid and were being directly affected by the thickness of the sediment layer near the bottom, and it is not surprising that the functional relationship is completely different. Though the top three points corresponding to the lowest values of ω also seems to plot reasonably well in the scaled figure 8, the deviations from the fitted line are in fact large, and it would probably be better to exclude them as being outside the range of conditions which can be fully explained.

6. Comparison with previous theories of particle suspension

6.1. *Numerical model of grid-stirred layers*

Noh & Fernando (1991*a*, *b*) have developed numerical models to describe dense turbulent layers stirred by a grid, for both a fluid layer with a stabilizing buoyancy flux and a layer of sedimenting particles. Though they introduce many detailed assumptions about the turbulent structure and the effects of density gradients on the turbulence, in

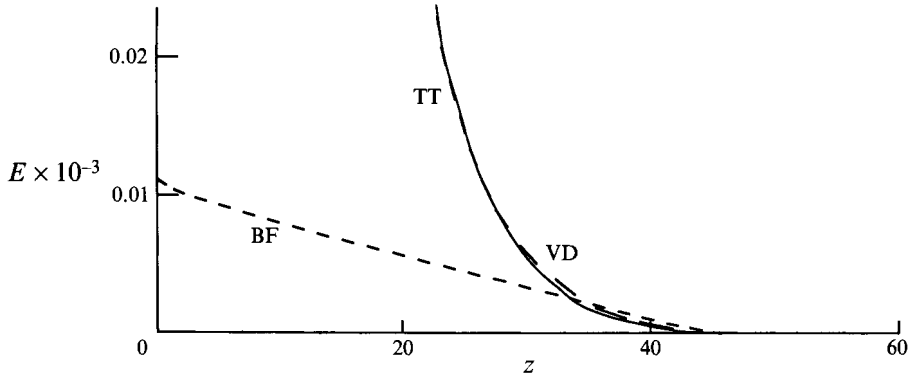

FIGURE 11. Comparison of the turbulent energy transfer (TT), the buoyancy flux (BF) and the viscous dissipation (VD) calculated by Noh & Fernando (1991*a*) as functions of distance from the 'stirring grid' in their numerical computation. Note that the BF dominates the energy balance near the final height, even though it is small there, since it falls off more slowly than VD.

essence the underlying physical processes are the same as those introduced by Hopfinger & Linden (1982) and E & Hopfinger (1987), as discussed in §4. In the present section we explore the similarities and differences between these treatments to shed further light on our experimental results and their interpretation.

First, we describe the fluid layer results and conclusions of Noh & Fernando (1991*a*) in a qualitative way before considering the particle case in more detail. They impose a constant buoyancy flux $B = B_0$ and a fixed input of turbulent kinetic energy $E = E_0 \propto u_0^2$ at the bottom of the computational region, and calculate the approach to a steady state. The equilibrium layers have a weak interior density gradient with a sharp density step above it, so that B decreases nearly linearly from B_0 at the base to zero at $z = D$, the top of the layer. However, E and the associated eddy diffusivity decrease to zero much faster than B, so that though the latter is small near D it nevertheless dominates the energy balance there compared to the viscous dissipation. This is shown in figure 11, reproduced from Noh & Fernando (1991*a*). The same features are seen in figure 10, calculated using the simpler model of Hopfinger & Linden (1982). The specific empirical dependence of eddy diffusivity on density gradient introduced by Noh & Fernando (1991*a*) emphasizes this effect and leads to the formation of a sharper front across which the propagation of both turbulent kinetic energy and the buoyancy flux are inhibited. But the formation of a layer of finite depth is an inevitable consequence of the rate of reduction of E by the buoyancy flux, as expressed by the ratio $\mathscr{F} = (u_0^3/B_0 z_0)$ used in the theory leading to figure 10.

We now turn to Noh & Fernando (1991*b*) which deals with suspensions. In this summary of their work some of the notation will be modified to take into account definitions already used in this paper. They introduce conservation equations of mass and momentum for both fluid and suspended particles, with the latter diffusing upwards and settling under gravity, and an equation for turbulent kinetic energy as a function of time and distance from the source. An eddy viscosity K^* and energy dissipation rate ϵ are defined in terms of the turbulent kinetic energy $E = u^2$ and integral lengthscale l_1 by

$$K^* = c_\mu E^{1/2} l_1 \quad \text{and} \quad \epsilon = c_D E^{3/2} l_1^{-1}. \tag{21}$$

The equations are made non-dimensional using a characteristic velocity scale u_0 and lengthscale z_0 (in our previous notation) and the particle concentration is scaled using

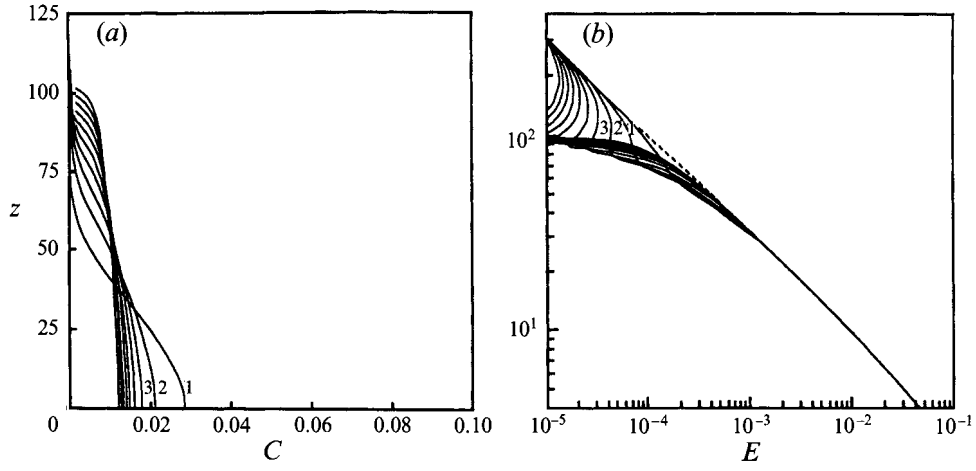

FIGURE 12. (*a*) The concentration of particles C and (*b*) the turbulent energy E calculated by Noh & Fernando (1991*b*) as functions of time (as marked on the graphs) and distance from the 'stirring grid', for $G = 10^{-3}, R = 10^{-3}$.

the total concentration in the layer of final depth z_∞, which is equivalent to the product $C_\infty z_\infty$ in the definition following (19*a*). (The downward buoyancy flux associated with this concentration is $g^* v_s C_\infty$, as defined in (17).) Noh & Fernando (1991*b*) then introduce the low-concentration limit in which l_1 is assumed to increase linearly with z and the r.m.s. turbulent velocity u is taken to be inversely proportional to z (cf. our equation (2)). They then modify these using empirical expressions to take account of the effect of stratification on these scales. For our present purposes it is important to note that these further complications change the detail but not the essence of the resulting solutions.

Two significant dimensionless parameters are then identified, namely

$$R = v_s/u_0, \tag{22}$$

The ratio of the particle fall velocity to the turbulent velocity scale, and (using the notation introduced in the present paper)

$$G = g^* C_\infty z_\infty / u_0^2 = g^* M_\infty / A \rho_P u_0^2, \tag{23}$$

which has the form of an overall Richardson number. The time-dependent equations are then solved for various combinations of R and G to trace the evolution of the turbulent kinetic energy and concentration fields in different circumstances.

In a series of calculations with fixed $G = 10^{-3}$ but different R, a sharp front is formed for $R = 10^{-3}$ and $R = 10^{-2}$ but not for $R = 10^{-1}$; in this last case the particles are evidently falling out too rapidly, and a gradient of concentration is set up in which diffusion and settling are in balance. When a front is formed the density gradient due to particles can be neglected below the front, but the energy decay due to the buoyancy flux is dominant in the turbulent energy equation at the level of the front, just as it is in the case of the fluid layer with a stabilizing buoyancy flux. The concentration and turbulent energy distributions for one of these cases are reproduced in figure 12. When R is held at $R = 10^{-2}$ and G is varied, no front forms with $G = 10^{-4}$ but it does form with $G = 10^{-2}$ when the buoyancy effect of the particles is larger.

We now turn to the dependence of the final layer depth z_∞ on R and G as determined by Noh & Fernando (1991*b*), and relate these to the earlier results. These authors use

a mechanistic argument following closely that of E & Hopfinger (1987) (which we have summarized in §4) to show that

$$z_\infty/z_0 = \text{const.}\, G^{-1/3}R^{-1/3}, \tag{24a}$$

and this dependence on both G and R is borne out by the detailed numerical results (with deviations from this for larger R when the extra effects of density gradients and so on are taken into account). Inserting the definitions (22) and (23), writing $u_0 = \omega d$ and identifying d with the lengthscale z_0 near the grid, we can express (24a) as

$$z_\infty = \omega d^2 (g^* v_s M_\infty / A\rho_P)^{-1/3}. \tag{24b}$$

This is the same form as our (19b) when the difference between the layer depth and the distance of its top from the grid is ignored. We note also that the product GR which occurs naturally in (24a) is a flux Richardson number, proportional to the inverse of the parameter $\mathscr{F}$ introduced in (15) and (16). Thus we find, not surprisingly, that with the same underlying physical assumptions the numerical results of Noh & Fernando (1991b) give the same functional forms as the theory already summarized.

6.2. *Criterion for the formation of a front*

We now consider the criterion deduced by Noh & Fernando (1991b) both numerically and analytically for the formation of a front (the existence of which we have assumed in the previous subsection). Provided R is small enough for the effect of stratification on the internal lengthscales to be neglected, they show that a front can form if

$$G > 2.2R^2 \tag{25a}$$

approximately, or

$$g^* M_\infty / A\rho_P v_s^2 > 2.2. \tag{25b}$$

This has the form of a Richardson number, but it is based on the properties and total mass in suspension of the particles alone, and not on the stirring grid or the turbulence it produces. Thus for a given particle density and size (hence fall velocity v_s) a certain minimum weight per unit area of particles must be held in suspension before a steady layer of limited depth can form. This further interpretation of their results was not pointed out by Noh & Fernando.

In order to understand this strikingly simple but somewhat puzzling result we rewrite G/R^2 in the more general form

$$G/R^2 = g^* \int C\,\mathrm{d}z/v_s^2, \tag{25c}$$

which can be evaluated for any concentration distribution. In the regime where this parameter is sufficiently small that there is no sharp layer, C is almost exponential and takes the form $C = C_b \exp(-v_s z/K)$, where C_b is the concentration at the base ($z = 0$) and K is the eddy diffusivity, assumed constant with depth. The integral in (25c) is then $C_b K/v_s$ so that (25c) can be written

$$G/R^2 = g^* C_b K/v_s^3 = B_0 K/v_s^4, \tag{25d}$$

where $B_0 = g^* v_s C_b$ is the particle buoyancy flux at the bottom of the tank. Thus we see that both the buoyancy flux and the stirring rate (through K) are implicitly included in (25c), and they are not irrelevant as the form (25b) at first suggests. We note also that because v_s is proportional to λ^2 there is a very sensitive dependence of G/R^2 on particle diameter λ (and hence the present development might need changing considerably to describe a situation with a broad distribution of particle sizes). Once a layer has formed, the concentration of particles within it is approximately uniform

and the integral in (25*c*) can be evaluated as $C_b z_\infty$. Inserting this result and (19) into (25*c*), we find that once the layer has formed

$$G/R^2 = (B_0 K'/v_s^4)^{3/4}, \tag{25e}$$

where K' is a constant similar in structure to K. Thus the quantity $B_0 K'/v_s^4$ is again an appropriate combination to describe this second regime, to which the system jumps when a critical value of the parameter G/R^2 is exceeded. This snap-through, sub-critical mode of instability is very familiar in other contexts though the detailed physical processes driving the instability are all different. For example, an elastic column under axial loading suddenly buckles and takes on a new shape when a critical value of the Euler parameter is exceeded, and laminar flow in a pipe becomes turbulent, with a different mean velocity profile, at a critical Reynolds number.

We should also now ask the question: is there a clear physical reason why this parameter is the unique combination which should determine the existence of a sharp layer? In deriving (19) we assumed that B_0 and K (equivalent to the grid action, or to the product ωd^2 we used earlier) are the only external parameters on which z_∞ can depend. To say whether a layer will form or not we need a third quantity describing the properties of an individual particle, as distinct from the bulk effect. If this is chosen to be v_s, then it follows that (25*d*) is the only dimensionless combination which can be formed from these three physically relevant quantities.

It is also instructive at this point to compare this phenomenon of layer formation with other situations where non-uniformities develop on a smooth density profile. This problem was first addressed theoretically in an oceanographic context by Phillips (1972), and it has more recently been reviewed and followed up in the laboratory by Ruddick, McDougall & Turner (1989). The common feature in all these studies is that there is a turbulent transport mechanism producing a vertical buoyancy flux which depends on the local density gradient, and is initially constant or smoothly varying with depth. If a local perturbation increases the static stability over a certain depth range, and this change in gradient reduces the 'diffusivity' of buoyancy more rapidly than the local gradient increases, then the local decrease in flux causes the gradient to increase further, and so the perturbation will amplify. Conversely, the flux is increased where the gradient is weakened, and the convergence of buoyancy near the interface causes a step-like structure to form. For smaller initial density gradients the flux can increase smoothly as the gradient is increased, with no tendency for layer formation. There will be a particular gradient separating these regimes, at which the buoyancy flux is a maximum.

An analogous behaviour is implicit in the various forms of equation (25), the criterion for layer formation in suspended sediments. With a given composition and size of solid particles, the only variable determining the behaviour is the total mass in suspension M_∞. As M_∞ (and hence the density gradient in the suspension) is increased from zero, the concentration gradient first decreases smoothly from a maximum at the base to zero at large z. At a particular value of M_∞, given by (25*b*), the concentration gradient becomes large enough to cause the flux of particles to decrease over some depth range. This perturbation is amplified, and a relatively well-mixed layer forms, bounded by a sharp interface across which the flux is zero.

6.3. *Settling and entrainment of particles in convective layers*

There has been a great deal of interest in the recent geological literature regarding the settling of crystals in convecting magmas, lava lakes or magma oceans, and the criterion for re-entrainment from the bottom boundary. It had previously been

assumed that in turbulent or unsteady convection, when the r.m.s. turbulent velocity is much greater than the settling velocity, then particles could be held in suspension indefinitely. Martin & Nokes (1988, 1989) showed, however, using laboratory experiments and a related theory, that particles can continue to settle through the viscous lower boundary layer in these circumstances, at a rate which is determined by the Stokes settling velocity and the particle concentration but is independent of the level of turbulence. At low concentrations the number of particles N held in suspension in a layer of depth h is given by

$$\mathrm{d}N/\mathrm{d}t = -v_s N/h \tag{26}$$

and thus N decays exponentially with time, provided no particles are re-entrained from the bottom boundary. Similar conclusions have been reached by hydraulic engineers and sedimentologists, for example Einstein (1968) and McCave (1970).

The experiments reported by Martin & Nokes were conducted using mainly cooling at the upper boundary, but heating at the bottom was added in a few runs. In one of these, that with the most viscous fluid and the smallest particles, re-entrainment into the plumes breaking away from the bottom boundary layer occurred, so that the particle concentration approached a steady finite value, rather than zero, at long times. We will consider in this section whether the re-entrainment mechanism into such convective flows can shed any light on the grid-stirred case of interest here.

Koyaguchi *et al.* (1990) conducted a series of experiments using a suspension of dense particles heated from below. The particles were initially distributed uniformly in water through the whole depth (20 cm) of the tank and allowed to settle. For very low initial concentrations the particles settled exponentially in time, as described by (26). With larger concentrations, however, a stable bulk density stratification was set up, with a dense convecting layer, laden nearly uniformly with particles, below a clear layer, which was also convecting due to the thermal transfer across the interface. These layers were separated by a stable interfacial region containing a gradient of particle concentration, partly compensated by an unstable temperature gradient. The temperature of the bottom layer increased and its density decreased with time. Eventually the bottom layer became unstable, and it overturned into the upper layer. This homogenized the temperature and concentration (but at a lower level because of the particle fallout) and the whole process began again, with the cycle being repeated several times.

Koyaguchi *et al.* (1990) produced a theoretical description of these processes which satisfactorily explained their data. We note here two extra points which are relevant in the present context. First, in none of their experiments was the bottom heating rate large enough to cause particles to be re-entrained, so that all particles eventually fell out and there was no possibility of a steady state being attained. Second, even if the heating rate were increased sufficiently for re-entrainment from the bottom to occur, it would not be possible to maintain a stable layer of hot dense suspension below cold fresh water. Heat could not be lost sufficiently rapidly through the bounding interface to prevent the net density of the lower layer decreasing and leading to overturn. We note too that in a thermally convecting layer the turbulent velocities increase as the layer depth increases, rather than decrease with distance from a stirring grid, and this is another factor militating against the formation of steady convecting layers stabilized with particles.

Another series of experiments, in which Koyaguchi, Hallworth & Huppert (1993) considered the case of cooling a suspension of particles from above, also sheds some light on these questions. For very dilute suspensions, convection maintained a

homogeneous distribution of particles, from which fallout occurred with a corresponding exponential decrease of N with time, as described above for bottom heating. Above a critical concentration, a descending sharp interface formed between a convecting upper clear very dilute region and a non-convecting lower region in which there was unimpeded sedimentation, with N decreasing at a linear rate.

Solomatov, Olson & Stevenson (1993) have briefly reviewed the above and other previous studies of convective suspensions, and have carried out a series of experiments to investigate the mechanisms and quantitative criteria for particle entrainment from the lower boundary. Before each run a suspension of small polystyrene spheres was allowed to settle in a tank containing salt solution, the density of which could be varied, to form a dense bed of about 2–3 mm in thickness. The temperature at the top of the 10 cm × 10 cm × 10 cm tank was held fixed, and a constant heat flux was supplied at the bottom. In each experiment the heat flux was changed in steps and the system allowed to come to a quasi steady state after each change in power. The conditions at which the bed motion and the entrainment began were noted, and the results plotted in two different ways, as suggested by two different possible mechanisms of entrainment.

Their first plot identified the parameters used for the analysis of turbulent shear flows, as will be discussed further below. The ratio of the Reynolds stress $\tau_* = \rho u_*^2$ to the weight per unit area of a particle $\Delta\rho g\lambda$ was plotted against the particle Reynolds number $Re_p = u_* \lambda/\nu$, where u_* is the friction velocity, λ is the particle diameter (using our notation, rather than theirs), g is the acceleration due to gravity, ν is the kinematic viscosity and ρ is the fluid density, and compared with data for the incipient motion of a bed under a turbulent shear flow. In turbulent shear flows the Reynolds stresses are the only stresses that can entrain particles, but Solomatov *et al.* concluded that these are not sufficiently large in convective flows to account for the bed motion and entrainment that both they and Martin & Nokes observed. In the case of convection, buoyancy stresses must be responsible for the entrainment, and these are much larger than the Reynolds stresses except at very large Rayleigh numbers.

The buoyancy stress τ_T is the viscous stress associated with the buoyancy flux from the lower boundary. In the laminar regime this is just $\eta u/d$, where η is the dynamic viscosity and u and d are the velocity and length scales of a simple one-scale flow. Solomatov *et al.* (1993) infer that the one experiment of Martin & Nokes (1989) which led to entrainment was in fact in the laminar regime. In the turbulent case, τ_T is the stress associated with the Komogorov scale, which can be expressed in terms of $\nu = \eta/\rho$ and the buoyancy flux F, which is proportional to the rate of kinetic energy production and hence to the energy dissipation, as

$$\tau_T/\rho = (\nu F)^{1/2}. \tag{27}$$

The plot of both sets of data in the form $\tau_T/\Delta\rho g\lambda$ against another particle Reynolds number (the latter now being conveniently defined in terms of the velocity and length scales at the edge of the thermal boundary layer) is reproduced from Solomatov *et al.* (1993) in figure 13. These buoyancy stresses are about an order of magnitude higher than the Reynolds stresses. It can be seen that entrainment in the Martin & Nokes (1989) laminar experiment was observed at approximately the same value of $\tau_T/\Delta\rho g\lambda$ as in the turbulent experiments. Thus it can be concluded that the buoyancy stresses are responsible for the entrainment from the bottom boundary in both laminar and turbulent convection.

Detailed observations by Solomatov *et al.* (1993) of the bed of particles in the experiments where entrainment occurred showed that the particles were swept into ridges or dunes by the thermal plumes and that particles were lifted and put into

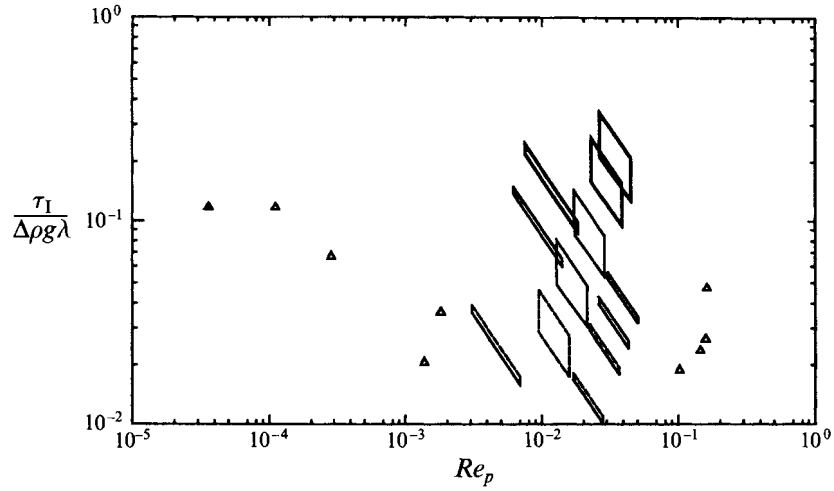

FIGURE 13. A reproduction of the plot presented by Solomatov *et al.* (1993) using coordinates appropriate for scaling with the thermal buoyancy stress. The ordinate is the ratio of the buoyancy stress to the weight per unit area of the particles, and the abscissa is a particle Reynolds number based on the velocity at the boundary layer height. The boxes outline error estimates based on the range of particle sizes and the uncertainty in the density measurements. Dotted outlines indicate no bed motion, solid lines strong motion of the entire bed surface, and heavy lines cases where entrainment did take place. The triangles represent Martin & Nokes' (1989) measurements, the solid symbol indicating the single experiment where entrainment was observed.

suspension off the crests of these dunes. This provides a much more effective mechanism than the entrainment of single particles vertically through a viscous sublayer. The horizontal stresses are much larger than direct vertical stresses near the solid boundary. The horizontal motion of particles and the associated convergence can create steep and high dunes at the base of plumes which are breaking away from the surface, so producing vertical velocities and stresses comparable with the horizontal values.

This mechanism and bed form can be compared directly with the observed sediment distributions under the stirring grids in our experiments described in §3. Since the grid bars are so close to the bottom, settled particles are swept sideways away from each bar, and when stirring is stopped, mounds of particles are observed to have accumulated in a square pattern between the bars. During stirring, a dynamic equilibrium must be established, with particles settling uniformly, being swept sideways by the horizontally deflected downward jets produced by the vertically oscillated bars, and then re-entrained from the tops of the mounds or dunes formed between the bars. The origin of the stress is then more akin to the Reynolds shear stress mechanism, since it is produced by a mechanical rather than a convective process.

Solomatov *et al.* (1993) also measured the equilibrium concentration of suspended particles for two values of the heat flux for which entrainment was observed. The concentration was in each case very small (less than about 0.1%), and they assumed that the particles could have had no effect on the turbulence in the convecting layer. The increase in suspended fraction was approximately proportional to the increase in heat flux. The interpretation of these measurements is not so firmly supported as their earlier conclusions, and it is also less relevant to our grid-stirred experiments so it will not be discussed further here.

6.4. *Suspension layers in channels, rivers and estuaries*

In very turbid waters, such as shallow estuaries or coastal water with unconsolidated mud on the bottom, field data show that the water column can be divided into a heavily sediment-laden bottom layer and a clearer top layer. These are separated by a sharp interface, called the lutocline. Wolanski *et al.* (1988) have summarized various observations of this phenomenon, and have shown that this distribution cannot be explained in terms of a simple balance between the upward eddy flux of particles, commonly assumed to be independent of the particle concentration, and the downward flux due to sedimentation, which leads to smoothly varying vertical profiles of suspended sediment concentration (SSC).

Wolanski *et al.* (1988) conducted a detailed observational program to study this process in the South Alligator River in northern Australia. We note immediately that the flow in this macrotidal river, in the dry season, was determined entirely by the tides, and that the sediment concentration had no effect on driving the quasi-horizontal water motions. At the measurement position the flood tide was significantly stronger than the ebb, and the SSC was clearly modulated by the tides. At flood tide there was no measurable vertical stratification of SSC when the currents exceeded 1 m s^{-1}. As the ebb tidal currents increased, a strong lutocline formed, starting from the bottom, with a two-layer flow persisting because of a difference in SSC; for most of the ebb the two layers were of comparable thickness.

These measurements are consistent with the idea that with very strong currents (at flood tides) the turbulence generated by the bottom stress can reach the surface and maintain a smooth profile of SSC, whereas for weaker currents the buoyancy gradients due to suspended sediment can damp the turbulence at a certain elevation. The numerical model set up by Wolanski *et al.* to describe this flow or, more generally, a quasi-steady flow in a channel containing sediment on the bottom, is again based on the mass conservation equation, with the fallout of particles balanced by upward diffusion, but with the important addition that the eddy diffusion coefficient K is now considered to be a strong function of the vertical density gradient, through a dependence on a Richardson number. They also assume that there is a saturation condition, or upper limit to the sediment concentration, implying that there is a maximum amount of sediment which can be entrained off the bottom.

In spite of the need to introduce a number of empirical assumptions, the basic physical ingredients of this model are very plausible, and they lead to robust predictions that a step structure will evolve, regardless of the particular assumptions made about $K(Ri)$. In considering the scaling laws for the interface height, however, the authors refer also to the paper of E & Hopfinger (1987) described in §4, and specifically to relation (10) (the Monin–Oboukhov length) for the depth of the suspension layer. This implies two things: first, that it is the balance between the kinetic energy input and the buoyancy *flux* determined by the fallout of particles which is determining the position of the lutocline, rather than a local gradient Richardson number criterion; secondly, that the appropriate turbulent velocity and length scales remain u_* and the layer depth, rather than those obtained by allowing for the decay of turbulence away from the boundary. The latter modification was required to describe grid turbulence, and led to (16).

In a further discussion of this model, Wolanski *et al.* (1989) suggested that a fast rate of erosion of bottom sediment would give a large effective negative buoyancy flux. This could limit the depth of the sediment layer more than the 'equilibrium' rate of lifting, which just balances settling. We can ask if such a transient initial state can go smoothly

to equilibrium when excess sediment remains on the bottom, or is the case where all the available sediment is suspended the only steady state? Is it possible that an oscillatory behaviour can develop, with excess sediment being picked up, damping the turbulence, and then being redeposited? Related questions will be raised in the following subsection, in the context of turbidity currents.

6.5. *Turbidity currents*

Turbidity currents differ from all the sediment-laden flows discussed above in one major respect: the flow responsible for producing the turbulence which keeps dense particles in suspension is generated by the buoyancy due to the particles themselves, as gravity drives the current down a slope. In the other cases considered the *generation* of the turbulence is independent of the sediment load, though in all of them, including turbidity currents, the level of turbulence is limited by the energy required to keep the particles in suspension.

Bagnold (1962) set out the principles of the argument using an energy argument in a way that has not since been matched for its clarity and simplicity. He supposed that a mass m per unit area of solids, of density ρ_P, is held in suspension in a fluid of density ρ, and forms a turbidity current moving down an inclined boundary with slope β. We denote the transport velocity down the slope of the fluid by $\bar{u}$ and of the solids by $\bar{U}$. Consider further that the particles are falling steadily at velocity v and are being lifted by the turbulence at the same rate in order to maintain a steady state. The power expended in lifting the particles and keeping the mass m at the same distance above the bed is then given by $(\rho_P-\rho)gmv/\rho_P = g^*mv$.

The power input due to the tangential pull on the particles in the direction of transport is $g^*m\bar{U}\sin\beta$. The net power contributed by the fluid motions in order to maintain the suspension is the difference.

$$\frac{\rho_P-\rho}{\rho_P} gm\bar{U}\left(\frac{v}{\bar{U}}-\sin\beta\right). \tag{28}$$

This is zero when

$$v = \bar{U}\sin\beta. \tag{29}$$

At this marginal condition the particles are just kept in suspension by the energy supplied by the flow. The sediment then suspends itself, in the sense that it requires no net energy expenditure by the fluid. This relation also implies that a particle settling and moving downslope at both the mean speeds will stay the same distance above the bed. Bagnold (1962) suggested that (28) has the important consequence that 'the mass m transportable by a given stream may therefore rise to an indefinite value, limited only by the availability of the solid material'.

Various more complex criteria for autosuspension have been suggested. Pantin (1979) and Parker (1982) have considered the time-dependent problem, and came to the conclusion that (28) should be regarded as a necessary but not sufficient condition. Pantin (1979) introduced an efficiency factor, which results in a substantial reduction in the estimate of the size of material a given flow can support. Stacey & Bowen (1988*a*, *b*) proposed that the vertical structure of a turbidity current, the interfacial stress and the entrainment of water from above, all need to be examined more closely, and related to gradient and bulk Richardson numbers describing the flow. They also deduced an auto-suspension criterion, which takes into account the vertical structure of the currents and depends on the bottom drag coefficient. This has the same form as (28) and Pantin's modification of it, and lies between the two in its quantitative predictions about the ease with which a turbidity current can maintain sediment in suspension. However, after surveying all the criteria which have been proposed,

Seymour (1990) came to the conclusion that Bagnold's criterion is not only the simplest but still the most satisfactory for explaining the available observations for self-sustained turbidity currents.

The most thorough treatment of variable turbidity currents is that presented by Parker, Fukushima & Pantin (1986). The aim of that paper was to evaluate the range of conditions under which a turbid underflow can pick up sufficient particles from the bed to maintain its motion down the slope. One conclusion which can be drawn from their calculations should be noted immediately: a 'steady state' having both constant downslope velocity U and constant rate of sediment transport per unit width $\psi = UCh$, where C is the concentration and h is the depth of the current, requires a very special balance between the competing processes of turbulence generation and particle suspension or fallout. It is in fact a state of unstable equilibrium, on one side of which the flow is subsiding and on the other it is 'igniting'. Relatively little attention has been paid to the former depositional regime, though Sparks *et al.* (1993) have treated the case of sediment-laden gravity currents with lighter interstitial fluid, for which sedimentation leads eventually to lift-off of the lighter components. Dade, Lister & Huppert (1994) have also recently presented a theory describing deposition from gravity-driven surges propagating down a slope and have begun to consider further the case of sustained gravity currents.

The analysis of igniting currents involves deriving and solving four coupled nonlinear equations for conservation of fluid, sediment, momentum and turbulent energy. These are related by an entrainment model linking the net amount of sediment lifted into the current to the vigour of the turbulent motions produced by the downslope flow. (It should be noted that, though Parker *et al.* 1986 numerical model incorporates many empirical assumptions and specific numerical values which may be questionable, we feel that the overall physical principles are robust and soundly based.) A distinctive feature of their model is the addition of a fourth equation for turbulent energy, to which the entrainment of sediment is linked. This provides a constraint on physically realistic solutions based on the other three conservation equations; when used without the energy constraint these imply such strong self-acceleration that the turbulent energy consumed in entraining extra sediment from the bed exceeds the supply of energy to the turbulence. Thus the turbulence, and hence the turbidity current, will grow and then die. The four-equation model again predicts self-acceleration, and the range of conditions under which this can occur, but it gives a much more modest rate of increase of velocity, with an acceleration which is sustainable in terms of the balance of turbulent kinetic energy. The numerical solutions reveal the possibility of a damped periodic behaviour in the early stages (starting with particular initial conditions), but this dies away and the acceleration remains smooth thereafter. In this quasi-equilibrium state, the overall Richardson number

$$g^*\psi/U^3 \tag{30}$$

stays nearly constant, implying that ψ is increasing like U^3. A similar behaviour was observed in the Ellison & Turner (1959) model for the approach to the 'normal' state of unsteady conservative fluid density currents, on which Parker *et al.*'s (1986) model is based.

The similarities between these calculations and our grid-stirring experiments will now be explored. In both studies the energy required to lift or keep particles in suspension is an important physical constraint, and the criterion for entrainment of sediment from the bottom is the crucial factor in each case. Our result that below a critical frequency ω_1 no particles can be maintained indefinitely in suspension has its

Quantity	Suspension mechanisms			
	Stirring grid	Convection	Channel flow	Turbidity currents
Eddy lengthscale	Increasing with distance from grid $\propto z$	Depth of layer	Depth of water *or* suspension layer	Depth of current
Velocity scale	Decreasing with distance above grid (powerlaw)	Increasing with depth of layer $\propto B^{1/3}z^{1/3}$	Proportional to mean velocity (set by pressure gradient)	Mean velocity (modification due to stratification. Velocity related to $\Delta\rho$)
Mechanism of turbulence generation	Directly by grid	Action of gravity throughout layer	Shear stress at boundaries	Shear at bottom boundary (also at interface on steep slopes)
Re-entrainment of particles from bottom?	Yes, depends on conditions below the grid	Only with strong bottom heating, by 'buoyancy stress'	Possible if shear stress is large enough	Yes, when shear stress is large enough
Possibility of steady-state layer of finite depth?	Yes, documented in our experiments	Not possible; intermittent overturn and eventual settling out	Yes, documented in estuaries	May be unstable: either settling *or* ignition on erodible bed

TABLE 2. Comparison of the properties of the turbulence, and the resulting layers of suspended particles, generated by the four mechanisms discussed in the text.

parallel in the behaviour of Parker *et al.*'s dimensionless 'sediment entrainment function' E_s. This is defined by $v_s E_s = F_b = \overline{c'w'}$, the volumetric Reynolds flux of suspended sediment at the bed, and it can be evaluated from empirical data on suspensions in open channel flows and in turbidity currents. The entrainment function E_s is zero for flows with a sufficiently small turbulence level. Beyond a critical level, which they define in terms of the friction velocity u_* and the particle Reynolds number, E_s increases extremely rapidly with u_*, until E_s saturates at a value of about 0.3 and there is no further increase in sediment entrainment with u_*. At this end of the range too there is a similarity with the grid-stirring experiments with the largest values of M_0, where our data suggest an approach to a self-limited condition in which the concentration is high and the layer depth small.

7. Conclusions and discussion

Our laboratory experiments and the associated theory have given an improved understanding of the conditions necessary for the formation of a suspension layer and its maintenance. We have studied in some detail the case of dense particles held in suspension by turbulent motions generated by an oscillating grid near the bottom of an experimental tank. For a given particle size and initial mass of particles in suspension, there is a limited range of stirring frequencies, and hence turbulent intensities, over which a given mass of particles can be held indefinitely in suspension in a layer of fixed depth. This equilibrium depth is described well as a function of the Stokes settling velocity of a single particle and the mass in suspension by the relation (20).

There is good agreement between the laboratory observations and a theoretical model based on a simple dimensional argument. The two essential external parameters entering this theory are the 'grid action' describing the turbulence, and the buoyancy flux associated with particles falling out and being lifted and held in suspension. The results cannot be explained simply in terms of the equivalent entraining fluid layers, for which experimental results have also been presented in this paper. The work done in keeping particles in suspension and the effect of this on the turbulence must be taken explicitly into account. Previous theories of this process have been extended, in order to reach a better understanding of the effect of the buoyancy flux on the turbulence.

The results of the stirring grid experiments cannot be directly taken over to other cases of practical interest, such as flowing layers of ash or snow particles, and the suspension of crystals or silt. The broad conceptual links are easy to make, but a quantitative comparison is not yet possible. We have discussed in this paper the current state of research on the various types of sediment-laden flows which can be identified, and have summarized the essential physical content of each of them. It will be helpful in conclusion to compare these results, and to suggest what cross-connections can be made, and which are inappropriate. In particular, we need to assess how the grid stirring results can be applied to sediment-laden channel flows and to turbidity currents.

Table 2 sets out the characteristics of the four kinds of particulate flows we have considered, and compares the properties of the turbulence, the mechanisms of its generation, and the effects of these on particle entrainment and layer formation. Turbulence generated directly by an oscillating grid differs from all the other cases in having an r.m.s. velocity which decays with distance from the bottom boundary. For channel flows and turbidity currents the scale remains proportional to the mean flow velocity when the flow is nearly homogeneous, though it can decay due to stratification or the energy loss associated with the suspension of particles. In convecting layers, the velocity actually increases with depth, and we believe this is the major factor in preventing the formation of stable, sediment-laden dense layers in a convective system heated from below. The eddy lengthscale increases with distance from the grid, whereas it is everywhere proportional to the total layer depth in the other cases.

The lifting of particles from the bottom in our experiments with a stirring grid depends in a sensitive manner on the geometry of the region below the grid, and in particular on the distance to the top of the sediment layer. But the mechanism of re-entrainment is a mechanical one, driven by the Reynolds stress acting on the bed of particles, and in this respect it is similar to the shear stress criterion that has been used to describe the entrainment of particles from the bed in channel flows or turbidity currents. Turbidity currents are unique among the flows considered in that there is an intimate coupling between the generation of turbulence and the amount of sediment in suspension; without a dense suspension layer driving the flow down a slope, there would be no energy to lift further particles.

Thus the flows to which our grid-stirred steady-state layer results should be most directly applicable are the sediment-stratified flows in estuaries. The detailed structure of the turbulence may be different, but the energetics of fallout and suspension are closely related. We note that such channel flows are most likely to become strongly layered during periods when sediment is being entrained rapidly from the bottom, with an associated large negative buoyancy flux. Turbidity currents have some features in common with these flows, but because of the strong coupling between the sediment concentration and the generation of turbulence, they are less likely to achieve a steady state. Unless the supply of erodible material is very limited, turbidity flows are either

depositing material or in a state of ignition where the particle load is continually increasing.

The stirring grid technique has great experimental advantages over the flow in a long channel, as a means of producing turbulence near the bottom boundary. Many further questions have been raised by the results of the experiments to date, and these should also be amenable to study using this technique in the future. There are, for example, the effects of hindered settling and polydisperse particle distributions, which could be important in nature, but which we have chosen not to address in this paper. In particular we intend to explore further the criteria determining the re-entrainment of particles by the flow near the grid. Once these have been established, it should be possible to carry out a more quantitative series of transient experiments and also to develop a theory of this regime.

We are grateful to R. C. Kerr, H. M. Pantin and a number of anonymous referees for helpful and penetrating reviews of an earlier draft of this paper. The reported research was supported by a number of grants from the NERC.

REFERENCES

BAGNOLD, R. A. 1962 Auto-suspension of transported sediment; turbidity currents. *Proc. R. Soc. Lond.* A **265**, 315–319.

DADE, W. B., LISTER, J. R. & HUPPERT, H. E. 1994 Fine-sediment deposition from gravity surges on uniform slopes. *J. Sed. Res.* A **64**, 423–432.

E, X. & HOPFINGER, E. J. 1986 On mixing across an interface in a stably stratified fluid. *J. Fluid Mech.* **166**, 227–244.

E, X. & HOPFINGER, E. J. 1987 Stratification by solid particle suspensions. *3rd Intl. Symp. on Stratified Flows, Caltech, Pasadena*, pp. 1–8.

EINSTEIN, H. A. 1968 Deposition of suspended particles in a gravel bed. *J. Hydraul. Div., ASCE* **94**, 1197–1205.

ELLISON, T. H. & TURNER, J. S. 1959 Turbulent entrainment in stratified flows. *J. Fluid Mech.* **6**, 423–448.

FERNANDO, H. J. S. 1988 Growth of a turbulent patch in a stratified fluid. *J. Fluid Mech.* **190**, 55–70.

FERNANDO, H. J. S. 1991 Turbulent mixing in stratified fluids. *Ann. Rev. Fluid Mech.* **23**, 455–493.

HOPFINGER, E. J. & LINDEN, P. F. 1982 Formation of a thermocline in zero-mean-shear turbulence subject to a stabilizing buoyancy flux. *J. Fluid Mech.* **114**, 157–173.

HOPFINGER, E. J. & TOLY, J.-A. 1976 Spatially decaying turbulence and its relation to mixing across density interfaces. *J. Fluid Mech.* **78**, 155–175.

HUPPERT, H. E., KERR, R. C., LISTER, J. R. & TURNER, J. S. 1991 Convection and particle entrainment driven by differential sedimentation. *J. Fluid Mech.* **226**, 349–369.

HUPPERT, H. E., TURNER, J. S. & HALLWORTH, M. A. 1993 Sedimentation and mixing of a turbulent fluid suspension: a laboratory study. *Earth Planet. Sci. Lett.* **114**, 259–267.

KITAIGORODSKII, S. A. 1960 On the computation of the thickness of the wind-mixing layer in the ocean. *Bull. Acad. Sci. USSR Geophys. Ser.* **3**, 284–287.

KOYAGUCHI, T., HALLWORTH, M. A. & HUPPERT, H. E. 1993 An experimental study on the effects of phenocrysts on convection in magmas. *J. Volcan. Geotherm. Res.* **55**, 15–32.

KOYAGUCHI, T., HALLWORTH, M. A., HUPPERT, H. E. & SPARKS, R. S. J. 1990 Sedimentation of particles from a convecting fluid. *Nature* **343**, 447–450.

LONG, R. R. 1978 A theory of mixing in a stably stratified fluid. *J. Fluid Mech.* **84**, 113–124.

MARTIN, D. & NOKES, R. 1988 Crystal settling in a vigorously convecting magma. *Nature* **332**, 534–536.

MARTIN, D. & NOKES, R. 1989 A fluid-dynamical study of crystal settling in convecting magmas. *J. Petrol.* **30**, 1471–1500.

McCave, I. N. 1970 Deposition of fine grained suspended sediment from tidal currents. *J. Geophys. Res.* **75**, 4151–4159.

Noh, Y. & Fernando, J. H. S. 1991*a* A numerical study on the formation of a thermocline in shear-free turbulence. *Phys. Fluids* A **3**, 422–426.

Noh, Y. & Fernando, J. H. S. 1991*b* Dispersion of suspended particles in turbulent flow. *Phys. Fluids* A **3**, 1730–1740.

Nokes, R. I. 1988 On the entrainment rate across a density interface. *J. Fluid Mech.* **188**, 185–204.

Pantin, H. M. 1979 Interaction between velocity and effective density in turbidity flow: phase-plane analysis, with criteria for autosuspension. *Mar. Geol.* **31**, 59–99.

Parker, G. 1982 Conditions for the ignition of catastrophically erosive turbidity currents. *Mar. Geol.* **46**, 307–327.

Parker, G., Fukushima, Y. & Pantin, H. M. 1986 Self-accelerating turbidity currents. *J. Fluid Mech.* **171**, 145–181.

Phillips, O. M. 1972 Turbulence in a strongly stratified fluid – is it unstable? *Deep-Sea Res.* **19**, 79–81.

Ruddick, B. R., McDougall, T. J. & Turner, J. S. 1989 The formation of layers in a uniformly stirred density gradient. *Deep-Sea Res.* **36**, 597–609.

Seymour, R. J. 1990 Autosuspending turbidity flows. In *The Sea* (*Ocean Engineering Science*) **9B**, 919–940.

Solomatov, V. S., Olson, P. & Stevenson, D. J. 1993 Entrainment from a bed of particles by thermal convection. *Earth Planet. Sci. Lett.* **120**, 387–393.

Sparks, R. S. J., Bonnecaze, R. T., Huppert, H. E., Lister, J. R., Hallworth, M. A., Mader, H. & Phillips, J. 1993 Sediment-laden gravity currents with reversing buoyancy. *Earth Planet. Sci. Lett.* **114**, 243–257.

Stacey, M. W. & Bowen, A. J. 1988*a* The vertical structure of turbidity currents and a necessary condition for self-maintenance. *J. Geophys. Res.* **93**, 3543–3553.

Stacey, M. W. & Bowen, A. J. 1988*b* A comparison of an autosuspension criterion to field observations of five turbidity currents. *Sedimentology* **37**, 1–5.

Thompson, S. M. & Turner, J. S. 1975 Mixing across an interface due to turbulence generated by an oscillating grid. *J. Fluid Mech.* **67**, 349–368.

Turner, J. S. 1968 The influence of molecular diffusivity on turbulent entrainment across a density interface. *J. Fluid Mech.* **33**, 639–656.

Turner, J. S. 1986 Turbulent entrainment: the development of the entrainment assumption and its application to geophysical flows. *J. Fluid Mech.* **173**, 431–471.

Wolanski, E., Chappell, J., Ridd, P. & Verlessy, R. 1988 Fluidization of mud in estuaries. *J. Geophys. Res.* **93**, 2351–2361.

Wolanski, E., Chappell, J., Ridd, P. & Verlessy, R. 1989 Reply to comments on 'Fluidization of mud in estuaries'. *J. Geophys. Res.* **94**, 6295–6296.